RESEARCH ARTICLE

Comparative finite element modelling of aneurysm formation and physiologic inflation in the descending aorta

Serena de Gelidi[a,b] and Andrea Bucchi[a]

[a] School of Mechanical and Design Engineering, University of Portsmouth, Portsmouth, United Kingdom; [b] Present address: School of Science & Technology, Middlesex University, London, United Kingdom

ABSTRACT
Despite the general interest in aneurysm rupture prediction, the aneurysm formation has received limited attention. The goal of this study is to assess whether an aneurysm may be instigated in a healthy model of an aorta inflated by a supraphysiological pressure. The effect of two main aspects on numerical predictions has been explored: i) the geometric design and ii) the constitutive law adopted to represent the material properties. Firstly, higher values of wall stress and displacement magnitude were generated in the physiologic model compared to the cylindrical one when assigning the same material properties. Secondly, greater deformations are observed in the anisotropic model compared to the isotropic one.

KEYWORDS
Fung; anisotropic; finite element; aorta; aneurysm

1. Introduction

Several finite element analyses have been carried out in order to predict the wall stress distributions in abdominal aortic aneurysms (Ma et al. 2007; Isaksen et al. 2008) and to evaluate their rupture potential (Raghavan and Vorp 2000; Giannoglou et al. 2006; Doyle et al. 2009). Despite the histological evidences, the arterial wall has been frequently modelled as isotropic (Delfino et al. 1997; Raghavan and Vorp 2000; Wang et al. 2002; Giannakoulas et al. 2005; Giannoglou et al. 2006; Isaksen et al. 2008; Scotti et al. 2008; Gasser et al. 2010; Wang and Li 2011; Shang et al. 2015). The arterial constitutive behaviour has been defined closer to being isotropic than anisotropic by Alhayani et al. (2013). On the other end, Schmidt et al. (2015) highlighted significant differences between the outcomes generated by an isotropic and an anisotropic model of a strongly idealized artery. Among the anisotropic formulations, even if the Holzapfel-Gasser-Ogden (HGO) model (Holzapfel et al. 2004) is often preferred (Badel et al. 2011; Rodríguez et al. 2008; Rodríguez and Merodio 2011; Alhayani et al. 2013), the Fung strain-energy function (SEF) (Fung et al. 1979) has recently been adopted to model the arterial wall (Sun et al. 2005; Ma et al. 2007; Avril et al. 2010; Lee et al. 2014). Ramachandran et al. (2012) discussed the most appropriate material modelling

choices to estimate the wall tension distribution, comparing Laplace law, Fung-type and isotropic polynomial strain-energy function (SEF). When the geometry is the only patient-specific information available, it has been concluded that the modelling choices have minimal impact on aneurysms wall tension evaluation (Ramachandran et al. 2012).

Finite elements simulations rarely focus on the understanding of how an aneurysm is instigated in arteries. As an example, Badel et al. (2011) simulated the inflation of a mouse carotid artery, modelled as a perfect cylinder, but no aneurysm was initiated. Historically, the topic of aneurysm formation in hyperelastic materials (Han 2007; Fu et al. 2012, 2008; Badel et al. 2013; Alhayani et al. 2013) has been addressed as a buckling problem from a macroscopic point of view. Han (2007) concluded that arteries may buckle and become tortuous due to the application of a high internal pressure even when the axial stretch ratio is below a certain value. The critical buckling pressure is proportional to the axial stretch ratio and to the wall stiffness (Han 2007). However, the arterial wall was modelled as thin and linear elastic. Fu et al. (2012) demonstrated that the aneurysm formation can be modelled as a bifurcation phenomenon induced by geometrical and material imperfections. In this study, the initiation pressure is defined by two main features. Firstly, the uniform inflation solution ceases to be stable as soon as the pressure reaches such value. Secondly, the near-critical bifurcated deformation is a bulge, of precisely the same form that has been observed experimentally (Fu et al. 2008). Lately, Lee et al. (2014) investigated the mechanical buckling and post-buckling behaviour of arteries in order to identify the inter-relationship between the artery buckling and aneurysms. They concluded that the shape and the curvature of the aneurysmal wall surface can lead to higher peaks in axial wall stresses, thus increasing the risk of an aneurysm rupture. Further studies focused on the buckling mechanisms leading to vessel tortuosity. Badel et al. (2013) showed that the tortuosity of veins is increased when their axial pre-stretch decreases and when their behaviour becomes more anisotropic. Alhayani et al. (2013) adopted the modified Riks method to instigate the bulge formation in isotropic, using Neo-Hookean SEF, and anisotropic, using Holzapfel-type SEF, arterial models. However, the material properties presented by Alhayani et al. (2013) appear to be idealised and not fully supported by an experimental test.

The aim of this study is to investigate the buckling of the descending aorta by assigning specific mechanical properties to the thoracic and abdominal regions. To the best of the authors knowledge, the combination of specific material properties along the same FE model of the arterial tree is novel as generally a single set of properties is assigned to the whole geometry. The mechanical behaviour of each district has been characterized by means of up-to-date techniques as presented in a previous work (de Gelidi 2016). Among the anisotropic models available in literature, the Fung SEF has been selected to model the experimental responses (Appendix). Differently from the HGO model, Fung SEF focusses on the phenomenological aortic behaviour, neglecting an explicit characterization of the fibres orientation. The dispersion and angle of fibres, required by the HGO model, need to be quantified by microscopic analyses that are beyond the aim of this research. Furthermore, given the limited attention reserved in literature, the application of the Fung model to study aneurysm formation is among the novelties of the present work. Two FE geometries have been designed to investigate the aneurysm appearance in a descending aorta: 1) a cylindrical idealised model and 2) a more physiologic one. Whilst each design features the same Fung orthotropic model parameters, the comparison between their predictions appears unique in literature. In order to predict any eventual elastic instability during inflation, the

modified Riks method (Riks 1979; Crisfield 1981) is adopted in a similar fashion as by Bucchi and Hearn (2013a,b) and Alhayani et al. (2013). This algorithm provides a load proportional factor (LPF) to be interpreted as a multiplier of the initial arbitrary load (pressure) applied to the lumen surface. Below the maximum LPF, the model deforms uniformly. The peak in the LPF value, instead, represents the critical pressure that causes the aneurysm formation, hence instability. Furthermore, in analogy to Schmidt et al. (2015), the same physiologic design has been described by means of a specific isotropic and anisotropic material properties aiming to investigate the effect of the material modelling choices on FE outcomes.

2. Materials and methods

2.1. Preliminary assumptions

Residual stresses (Chuong and Fung 1986; Vaishnav and Vossoughi 1987) were not measured, analogously to Deplano et al. (2016). Material parameters taking into account residual stresses were found to be not significantly different from the ones neglecting them (Labrosse et al. 2009). Furthermore, the stress in the load-free configuration, in which the arterial wall is not subjected to any loads, is assumed to be negligible (Raghavan and Vorp 2000; Wang et al. 2002; Georgakarakos et al. 2010). Accordingly, the same assumption has been made for the models presented in this investigation.

In addition, although the aorta consists of three layers (Holzapfel et al. 2000; Drake et al. 2010), only a single layer (Doyle et al. 2007; Badel et al. 2011; Maher et al. 2012; Lee et al. 2014) has been modelled in the present study. This choice is consistent with the experimental methodology adopted by de Gelidi (2016), since the layers have not been tested separately. Thus, the overall response of the aortic samples has been assigned to the computational model of the entire wall.

In order to isolate the effect of the pressure, the ageing of the tissue has been neglected. Finally, no contact with the spine and organs is taken into account in the simulations.

2.2. FE geometries

Two designs were generated, both intended as a simplification of a descending aorta. A graphical outline of the designs is displayed in Figure 1.

[Figure 1 about here.]

The first model consists into a cylindrical hollow geometry of which the total length is 335 mm. The internal diameter measures 20 mm and its wall thickness is equal to 1.64 mm along the whole geometry. Such value of thickness has been obtained in a previous study (de Gelidi et al. 2017). The material properties (Section 2.3) of the upper half of the model refer to the thoracic aorta, instead the behaviour of the inferior sector to the abdominal aorta. Such discontinuity of material properties appears not easily avoidable. After a sensitivity study, a mesh of 21376 C3D8H elements (Rodríguez et al. 2008; Fehervary et al. 2016), 64 in circumferential direction and 334 in longitudinal direction (equally distributed in the thoracic and abdominal segment), is generated. Since the present work does not focus on the gradient of stress generated across the wall, a single element was assigned for each model across the arterial wall. Although

it is uncommon in the literature to report the number of elements for each direction, Takizawa et al. (2010) observed comparable results using one or two elements across the thickness. However, mesh convergence tests have been carried out to compare the maximum stress obtained when one, two, three or four elements mesh the wall thickness.

The second model is conceived as a more realistic human descending aorta. The values of length, diameter and wall thickness adopted for this design refer to a data set originally tabulated by Noordergraaf (1956) and successively updated, for the lower abdominal aorta, by Westerhof et al. (1969). Recently, Wang and Parker (2004) adjusted such dimensions to produce a realistic human arterial tree. Thus, according to the nomenclature presented in Wang and Parker (2004) the following segment of the arterial tree were adopted: Thoracic aorta I and II, Abdominal aorta I to IV. All the details are reported in Table 1.

[Table 1 about here.]

As a result, a tapering of the aorta from the thoracic to abdominal district can be appreciated as both the diameter and the thickness progressively decrease. The total length (335 mm) matches the idealised cylindrical model. However, the thoracic sector (156 mm) is shorter than the abdominal one (179 mm). Once again, specific material properties are assigned to each region. A mesh of 21440 C3D8H elements is generated, 64 elements in circumferential direction and 335 in longitudinal direction (in the specific 156 for the thoracic segment and 179 for the abdominal).

2.3. Anisotropic material model

The material properties assigned to the Fung orthotropic formulation in Abaqus are based on the parameters obtained from the fitting procedure described in a previous work (de Gelidi 2016). In Abaqus (v. 6.14, Dassault Systèmes S.A., France), the generalized Fung strain-energy potential has the following form:

$$W = \frac{C}{2}\left[e^{Q(E)} - 1\right] + \frac{1}{D}\left(\frac{J_{el}^2 - 1}{2} - \ln J_{el}\right) \tag{1}$$

where C and D are the temperature-dependent material parameters and J_{el} is the elastic volume ratio, which is assumed to be 1 for an incompressible material. The initial bulk modulus K_0 depends on the initial deviatoric elasticity tensor D as follows

$$K_0 = \frac{2}{D}. \tag{2}$$

In order to define the full incompressibility, the *hybrid* formulation has been adopted and the parameter D has been set as nil for all the following models (Dassault Systèmes 2014).

Experimental data, collected from biaxial tensile tests (de Gelidi 2016), have been postprocessed by means of Matlab. The mathematical modelling of hyper-elastic materials requires the accurate identification of the fitting parameters from suitable experimental datasets. In order to describe the mechanical properties of the tissues, a nonlinear regression has been performed to model the experimental data by the Fung model (Eq. A1 and A2 in the Appendix). The fitting coefficients generated from this procedure are listed in Table 2 for the abdominal tissue and in Table 3 for the thoracic one.

4

The complexity of such fitting consists in taking into account three different stress-strain curves, which refer to the biaxial response in circumferential and longitudinal direction, coupled with a simple shear response (Appendix). The quality of the fitting is affected by the SEF convexity requirement, which demands that all Fung parameters need to be strictly positive (Holzapfel 2006).

[Table 2 about here.]

[Table 3 about here.]

A variety of recommendations is available in the literature to verify the stability of the Fung material and its physically meaningful mechanical behaviour (Sun and Sacks 2005; Pandit et al. 2005; Holzapfel 2006; Fan and Sacks 2014).
The convexity has been checked by plotting the contours in the Green-Lagrange strain planes (Holzapfel et al. 2000; Sun and Sacks 2005; Holzapfel 2006; Anssari-Benam and Bucchi 2017) representing the states of constant energy of the Fung SEF based on the coefficients listed in Tables 2 and 3.

2.4. Isotropic material model

Average stress-strain responses, collected by means of uniaxial tensile tests in a previous study (de Gelidi et al. 2017), have been adopted to describe the isotropic material properties of the thoracic and abdominal segment respectively in the physiologic design. The SEF by Marlow (2003) describes such data integrating the nominal uniaxial stress $\tau_1(\epsilon)$ over the strain interval $[0,\epsilon^*]$:

$$W(\epsilon) = \int_0^{\epsilon^*} \tau_1(\epsilon) \, \mathrm{d}\epsilon. \tag{3}$$

Differently from others constitutive models (e.g. (Ogden 1972), (Yeoh 1993)), it has been shown that Marlow SEF was the only one suited to predict aneurysm formation for this set of data (de Gelidi et al. 2017).

2.5. Boundary conditions

A supra-physiologic state, for which the arterial wall is subjected to internal pressures higher than the normal blood pressure (Schmidt et al. 2015), is used to study the case of aneurysm formation. The aneurysm formation is instigated by means of the modified Riks method (Riks 1979; Crisfield 1981) while an internal inflating pressure with a starting value of 1 kPa is applied. No axial pre-stretch was applied to simulate the worst case scenario: the pre-stretch, normally ensuring arterial stability (Rachev 2009), rapidly decreases with ageing (Horný et al. 2014). This condition is relaxed in order to increase the likelihood to predict aortic buckling, hence both ends were constrained for axial displacement.
Furthermore, in order to compare the FE outcomes computed by each design, a static inflation, intended to simulate a systolic pressure load, up to 16 kPa ($\sim$ 120 mmHg) has been performed.
All simulations were carried out by means of Abaqus (v. 6.14, Dassault Systèmes S.A., France).

3. Results

Contrasting outcomes in the aneurysm generation were achieved while characterizing the material with different strain energy functions. With the use of the orthotropic Fung model, no critical pressure and bulge appearance are computed for the cylindrical geometry (Section 2.2). Similarly, no aneurysm formation has been computed in the physiologic geometry. On the other end, the modified Riks analysis predicts in such design the aneurysm appearance at a critical pressure of 22.8 kPa ($\sim$ 171 mmHg) if the tissue is modelled as isotropic (Section 2.4). The formation is expected in the superior part of the abdominal aorta, where wall stress values exceed 1.3 MPa, as shown in Figure 2. It should be also noted that, as shown in Table 1, the thickness to radius ratio does not increase monotonically from the abdominal aorta I to the IV section.

[Figure 2 about here.]

The static inflation allows a comparison of the predictions of the two FE geometries (Section 2.2). As a result, larger deformations are achieved in the physiologic model, where the maximum radial displacement (10.91 mm) is higher compared to the maximum predicted for the cylindrical model (8.76 mm). Wall stress values on the external surface appear about 0.38 MPa higher in the thoracic physiologic model (Figure 3 A) compared to the thoracic cylindrical one (Figure 4). However, while the stress field is almost uniform in both thoracic regions and in the abdominal region of the cylindrical model, the stress in the physiologic abdominal aorta covers a range of approximately 0.2 MPa.

[Figure 3 about here.]

[Figure 4 about here.]

As a second main comparison, the effect of different material properties is studied in the same geometry: the physiologic design. As a result, the static inflation generates stress values comparable in both the isotropic and the anisotropic material models on the external wall surface of the abdominal area. In the thoracic region, the anisotropic model shows a stress about 52% higher than the isotropic one on the external wall. However, an even increased discrepancy between the models can be observed in the cutaway view, where lumen stress values appear more uniform and lower in the isotropic model compared to the anisotropic one (Figure 5). In the anisotropic model a gradient of von Mises stress of about 0.6 MPa can be observed across the lumen surface between the thoracic and abdominal area. Lastly, in the isotropic model the radial displacement does not exceed 6 mm, while in the anisotropic model this appears almost doubled ($\sim$ 11 mm).

[Figure 5 about here.]

4. Discussion

The literature suggests that uniaxial and planar biaxial tests are sufficient, but not complete, for characterisation of the aortic tissue and to model its anisotropic

6

behaviour by means of the Fung SEF. However, no work to date has published a complete set constitute of 9 parameters to fit soft tissue behaviour.

Schulze-Bauer et al. (2002) reported 4 parameters to fit the response of human femoral arteries subjected to inflation tests. In 2003, Schulze-Bauer and Holzapfel (2003) modelled already published clinical data of the thoracic aorta, oblivious of the cross-sectional area, by means of 4 Fung parameters. Sun and Sacks (2005) aimed to produce clear guidelines to build a Fung model in Abaqus. However, they published only 7 parameters. Pandit et al. (2005) published 4 coefficients to fit the experimental data obtained from the inflation tests performed on porcine left anterior descending artery. In 2006, Vande Geest et al. (2006) were unable to fit the experimental data with a 4 parameter Fung elastic model. Differently, Horný et al. (2006) fitted the responses of inflation tests on human thoracic aorta by means of 4 Fung parameters. However, they added a Neo-Hookean term to the SEF. Ma et al. (2007) claimed that their Abaqus model of cerebral aneurysm is modelled by 5 Fung parameters. In 2010, Avril et al. (2010) modelled in Abaqus the inflation of human arteries, publishing only 4 parameters. Vychytil et al. (2010) reported the 9 parameters equation, but they published only 6 coefficients with no assumption for the shear terms. Bellini et al. (2011) reported 4 parameters to fit the responses of planar biaxial tests conducted on the porcine duodenum, the jejunum and the ileum. Recently, Lee et al. (2014) published 7 parameters for porcine carotid arteries.

The present work arises no doubt that 4 Fung parameters are sufficient to obtain an excellent fit of biaxial tests results. In addition, the 3 parameters referred to shear are generally neglected in literature. Since no shear is generated during a simple inflation test (Vossoughi and Tözeren 1998), such parameters were initially disregarded in this work. However, it has been noticed that a sufficient material description requires 9 positive parameters for the orthotropic model. Thus, it is difficult to justify why no complete set of coefficients have been published so far, since they are necessary to run the FE model.

Therefore, the results in Tables 2 and 3 represent a considerable novelty.

The use of different elements has been explored for meshing the geometries. However, convergence has been reached only in the cylindrical design whether C3D8RH elements were employed in conjunction with fully constrained ends. Differently, incompatible mode hybrid elements (C3D8IH) ensured convergence in the physiologic model if the radial displacement is permitted. However, Abaqus guide recommends incompatible elements to improve the bending behaviour of regular displacement elements (Dassault Systèmes 2014).

The comparison between different geometries highlighted the larger deformations achieved in the physiologic model as a result of the static inflation. Furthermore, while the abdominal segment accounts for the highest stretch in the physiologic model, the stretch peak in the cylindrical model is expected along the junction between the aortic segments. Comparing the cylindrical and the physiologic models of descending aorta, higher wall stress values are reached, in both cases, in the thoracic district compared to the abdominal one. The range of values predicted in the stress field (~ 0.2 MPa) is suggested to be mainly a direct effect of the geometry, due to the decreasing diameter and thickness. In contrast with Takizawa et al. (2010), the results also suggest the use, in future studies, of multiple elements across the wall thickness due to the stress difference observed between the lumen and the external surface (Figure 3). The effect of the number of elements has been

quantified in Figure 6, which compares the wall stress values predicted by assigning 1, 2 or 4 elements across the thickness. No significant difference in stress values is appreciable for the isotropic material model. Such analysis has been extended also to the aneurysm instigation, which predicted a 0.08% scatter between the use of 1 or 4 elements in the cylindrical geometry and 0.04% in the more realistic geometry.

[Figure 6 about here.]

The comparison between isotropic and anisotropic material properties on the physiologic geometry revealed a substantial difference: the aneurysm formation was predicted only for isotropic material properties. This outcome represents the main novelty of the present work. The computed critical pressure of ~ 171 mmHg is a value of high systolic blood pressure that leads to a diagnosis of hypertension. Such condition affects more than one in four adults in the UK (NHS 2019), while the Abdominal Aortic Aneurysm (AAA) was detected in below 4% of men screened in 2017/18 (Public Health England 2019). Although the NHS states that high blood pressure can double the risk of getting a AAA (NHS 2017), the authors suggest that the aneurysm formation predicted by the isotropic model is a misleading outcome resulted by simplified material properties. Such findings appear in contrast with Ramachandran et al. (2012), who claimed that the modelling choices (Fung-type or isotropic) have minimal impact on wall tension evaluation. Similarly, Alhayani et al. (2013) observed that the formation of the bulge in the anisotropic (HGO) model appeared analogous to the one predicted in the isotropic design. However, their material properties were not fully corroborated by experimental data.

It is worth highlighting that, differently from other FE models, the specific mechanical behaviours of the thoracic and the abdominal aorta are contiguous in the model. Joining two different and specific biological responses is an aspect rarely addressed in literature, that appears novel for the Fung formulation. Such an approach highlighted, for the first time, the significant difference in terms of stress between the regions (Figure 2 and 4). Nonetheless it has been possible to predict the aneurysm formation for the isotropic model in the superior part of the abdominal aorta, which clinical incidence is far higher compared to the thoracic area. Although a local discontinuity in stress values is observed where different material properties connect, the overall results appear to be independent from such aspect. Furthermore, the gap of the predicted wall stress values between the isotropic and anisotropic models is likely the result of a different calibration. In other words, different experimental data have been embedded in each set of properties: uniaxial tensile test results have been used for the isotropic model, while these were complemented with biaxial tensile test and *synthetic* shear test outcomes for the Fung model. Due to the nature of the test, biaxial tensile tests generate softer responses compared to the uniaxial analyses.

Among the limitations of the present investigation, the experimental data refer to porcine aortic tissue. Hence, FE simulations related to the human tissue could lead to different outcomes. Although the physiologic design appears closer to the *in vivo* structure, no arteries connected to the aorta have been considered. As suggested by the present work, a different geometry may lead to different predictions. Despite the fact that haemodynamic forces are thought to be the main instigators on aneurysm formation and growth (Signorelli et al. 2018; Koseki et al. 2019), their influence has not been considered in this work. Since no dedicated facility was available, the shear re-

sponse, needed for anisotropic FE models, has been estimated analytically (Appendix). Thus, such results could differ from what could be observed in an experimental procedure alike the study presented by Sommer et al. (2016), who investigated the shear properties of a diseased thoracic aorta.

5. Conclusions

Material properties strongly affect the FE predictions, since the Fung orthotropic model generates quite distinct predictions compared to the isotropic one. Such difference is even enhanced in the aneurysm prediction, as only the isotropic model predicts an aneurysm formation. Such outcome could be especially valuable for studies aiming to predict the evolution of a patient-specific aorta into a possible aneurysm, as an isotropic model may mislead the prognosis.

Therefore, the present study suggests that an aneurysm formation in healthy models of aortas is unlikely to be caused by supra-physiologic pressure loading. Whether an aneurysm is predicted in the descending aorta, it is suggested that the abdominal district is more prone to show the bulge compared to the thoracic one. This is presumed to happen due to the combination of the material properties and the geometry, as both its diameter and thickness decrease substantially in the abdominal region.
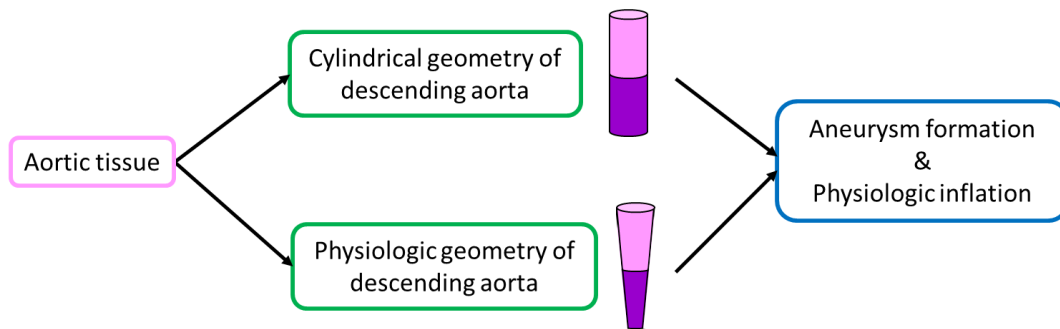
List of Figures

Figure 1. Schematic outline of the FE analyses performed for anisotropic models of aorta. Pink geometries are characterized by material properties of thoracic aorta, while purple ones refer to abdominal aorta

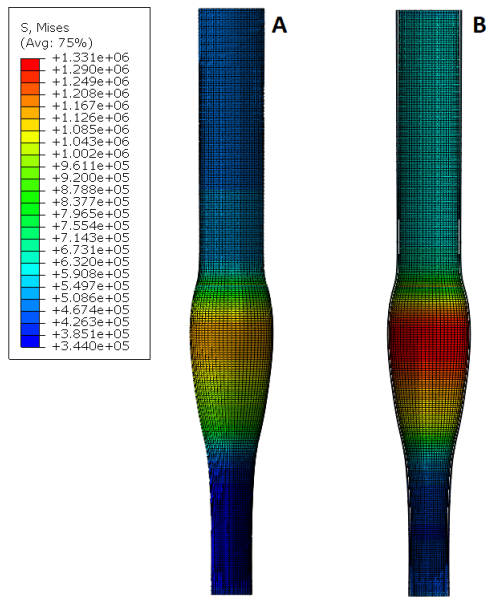**Figure 2.** Aneurysm formation predicted by the modified Riks method at a critical pressure of 22.8 kPa in a isotropic model of descending aorta. The upper district of the geometry is modelled by thoracic material properties, while abdominal material properties are assigned to the inferior district. Higher von Mises stress [Pa] levels are experienced on the internal surface of the geometry (B) compared to the external one (A)

Figure 3. von Mises stress [Pa] predicted for an anisotropic model of descending aorta subjected to a static inflation of 16 kPa ($\sim$ 120 mmHg). The upper region of the physiologic geometry is modelled by thoracic material properties, while abdominal material properties are assigned to the inferior region. Higher stress levels are experienced on the internal surface of the geometry (B) compared to the external one (A)
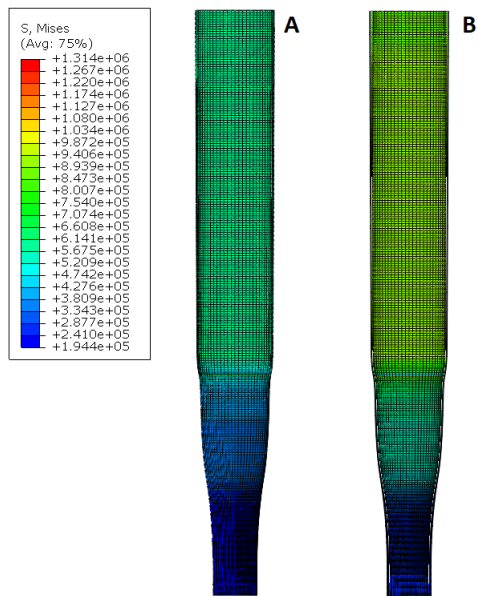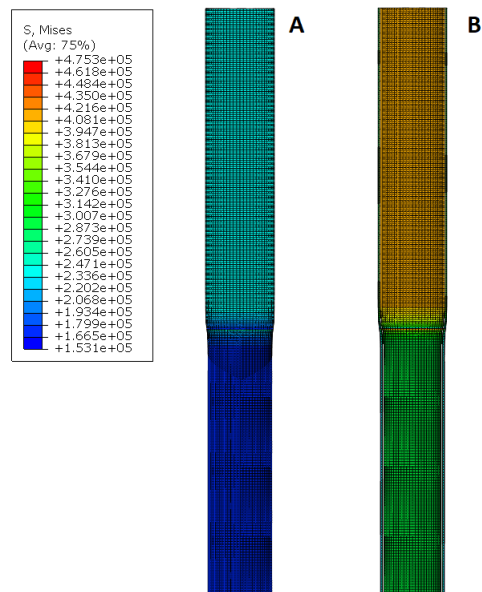
Figure 4. von Mises stress [Pa] predicted for an anisotropic model of descending aorta subjected to a static inflation of 16 kPa ($\sim$ 120 mmHg). The upper half of the cylindrical geometry is modelled by thoracic material properties, while abdominal material properties are assigned to the inferior half. Stress levels are predicted to be almost doubled on the internal surface of the geometry (B) compared to the external one (A)

14
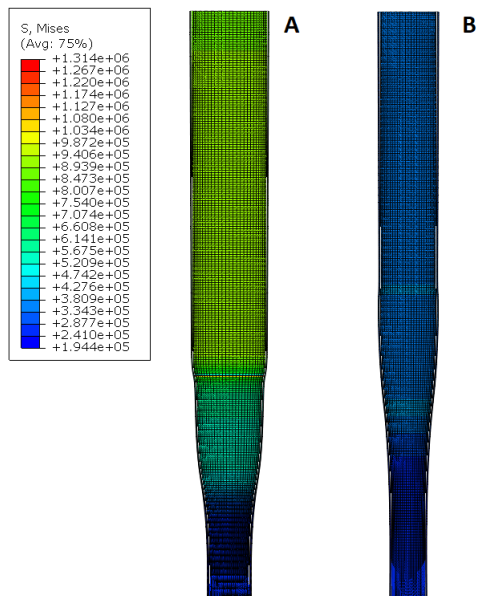
Figure 5. Comparison of von Mises stress [Pa] predicted for an anisotropic (A) and isotropic (B) model of descending aorta subjected to a static inflation of 16 kPa ($\sim$ 120 mmHg). The cutaway views highlight the different gradient of stress between the models, which is enhanced in the lumen surface compared to the external one as shown in Figure 3.

15
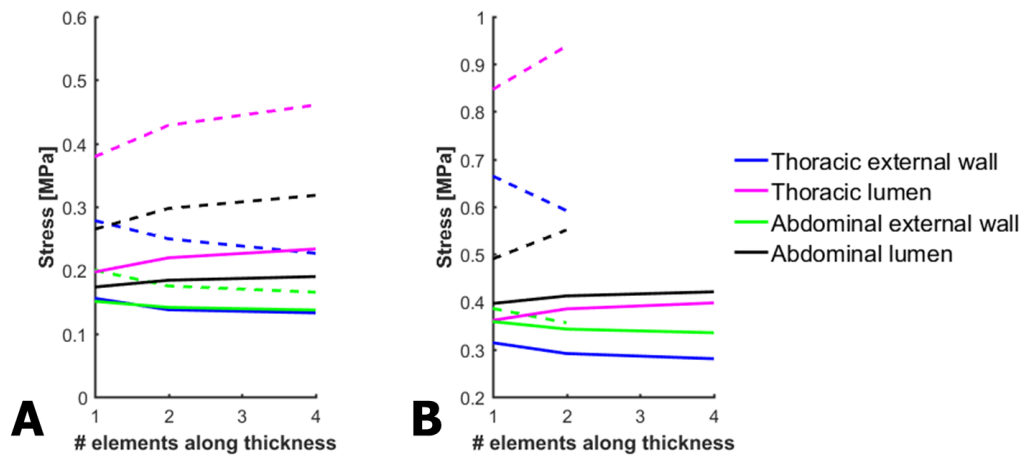
Figure 6. Mesh sensitivity evaluated for the inflation at 16 kPa ($\sim$ 120 mmHg) of the anisotropic (dashed) and the isotropic (solid) material model for the two FE geometries: A) the cylindrical and B) the more realistic human descending aorta. No convergence was reached for the anisotropic material model featuring 4 elements across the realistic geometry (B)

List of Tables

Segment	Length [cm]	Radius [cm]	Thickness [cm]	Ratio* [ ]
Thoracic aorta I	5.2	1.120	0.110	0.098
Thoracic aorta II	10.4	1.071	0.100	0.093
Abdominal aorta I	5.3	0.920	0.090	0.098
Abdominal aorta II	1.0	0.843	0.080	0.095
Abdominal aorta III	1.0	0.794	0.080	0.101
Abdominal aorta IV	10.6	0.665	0.075	0.113

Table 1. Geometric details adopted from Wang and Parker (2004) to design the realistic human descending aorta. *Ratio* is defined as the thickness divided by the radius.

Table 2. Fitting coefficients based on the experimental mechanical response of abdominal aorta subjected to uniaxial, biaxial and simple shear tests. Parameter C is expressed in Pa, while a_i are dimensionless

Fung parameter	Fitting coefficient
a_1	0.81
a_2	0.74
a_3	1.41
a_4	0.43
a_5	0.000035
a_6	0.0006
a_7	0.9
a_8	1.23
a_9	1.23
C	73277.87

Table 3. Fitting coefficients based on the experimental mechanical response of thoracic aorta subjected to uniaxial, biaxial and simple shear tests. Parameter C is expressed in Pa, while a_i are dimensionless

Fung parameter	Fitting coefficient
a_1	0.45
a_2	0.53
a_3	3.19
a_4	0.09
a_5	0.0003
a_6	0.002
a_7	0.51
a_8	7.58
a_9	0.13
C	73131.96

Appendix A.

According to Fung et al. (1979), the three-dimensional stress-strain behaviour of a soft tissue can be described by the following function

$$W = \frac{C}{2}[e^{Q(E)} - 1] \tag{A1}$$

where Q is expressed in terms of the Green strain E:

$$\begin{aligned} Q(E) = a_1 E_{\theta\theta}^2 + a_2 E_{ZZ}^2 + a_3 E_{RR}^2 + 2a_4 E_{\theta\theta} E_{ZZ} + 2a_5 E_{ZZ} E_{RR} \\ + 2a_6 E_{\theta\theta} E_{RR} + a_7 E_{\theta Z}^2 + a_8 E_{\theta R}^2 + a_9 E_{ZR}^2. \end{aligned} \tag{A2}$$

In order to estimate parameters a_7, a_8 and a_9 it is necessary to take into account shear behaviour, which cannot be captured by a biaxial tensile test in which the sample is aligned with circumferential and longitudinal directions Zhou and Fung (1997). Therefore, theoretical shear stress value are calculated as:

$$S_{\theta Z} = \frac{\partial W}{\partial E_{\theta Z}} = (2a_7 E_{\theta Z}) \frac{C}{2} e^{Q(E)} \tag{A3}$$

Green-Lagrange shear strain and stress data have been determined by means of *synthetic* simple shear test. The principal stretches for this test Horgan and Murphy (2010) are the following:

$$\lambda_1 = \frac{k}{2} + \sqrt{1 + \frac{k^2}{4}} \qquad \lambda_2 = \frac{1}{\lambda_1} \qquad \lambda_3 = 1 \tag{A4}$$

where κ is the amount of shear. As a result, the Green-Lagrange shear strain Vossoughi and Tözeren (1998); Fung (1993) is calculated as

$$E_{12} = \frac{1}{2}\lambda_1\lambda_2 \cos(\phi_F) = \frac{1}{2}\lambda_1\lambda_2 \cos\left(\frac{\pi}{2} - \phi\right) \tag{A5}$$

where ϕ and ϕ_F are the angles showed in Figure A1. The angle ϕ is worked out from the amount of shear κ Ogden (1997); Horgan and Murphy (2010)

$$\kappa = \tan(\phi) = \lambda_1 - \frac{1}{\lambda_1}. \tag{A6}$$

Once principal stretches from Equation A4 are substituted, the shear strain becomes

$$E_{12} = \frac{1}{2} \cos\left(\frac{\pi}{2} - \arctan(\kappa)\right). \tag{A7}$$

[Figure 7 about here.]

As the Cauchy stress in simple shear tests Nunes and Moreira (2013) can be expressed as

$$\sigma_{12} = 2\kappa \frac{\partial W}{\partial I_1}, \tag{A8}$$

where I_1 is the first invariant, defined as $I_1 = \lambda_1^2 + \lambda_2^2 + \lambda_3^2$ Horgan and Murphy (2010). Biaxial data are fitted by Yeoh SEF Yeoh (1993) in Abaqus as it is dependent on the first invariant and provides a good fitting of the experimental data. Thus, the fitting coefficients C_{10}, C_{20} and C_{30} are determined and Equation A8 becomes

$$\sigma_{12} = 2\kappa \left[C_{10} + 2C_{20}(I_1 - 3) + 3C_{30}(I_1 - 3)^2 \right]. \tag{A9}$$

Hence, a synthetic set of data for simple shear can be generated. The Cauchy stress (σ) is related to the second Piola-Kirchhoff (S) by Equation A3 as $\mathbf{S} = J\mathbf{F}^{-1}\sigma\mathbf{F}^{-T}$, from which $S_{12} = \sigma_{12} - k\sigma_{22}$. However, in the hypothesis of plane stress the normal component of the traction on inclined surfaces (σ_{22}) and σ_{33} are equal to zero Nunes and Moreira (2013). As a result, σ_{12} coincides with S_{12}.

References

Alhayani AA, Giraldo JA, Rodríguez JF, Merodio J. 2013. Computational modelling of bulging of inflated cylindrical shells applicable to aneurysm formation and propagation in arterial wall tissue. Finite Elements in Analysis and Design. 73:20–29. Available from: `http://dx.doi.org/10.1016/j.finel.2013.05.001`.

Anssari-Benam A, Bucchi A. 2017. Modelling the deformation of the elastin network in aortic valve. Journal of Biomechanical Engineering. Available from: `http://biomechanical.asmedigitalcollection.asme.org/article.aspx?doi=10.1115/1.4037916`.

Avril S, Badel P, Duprey A. 2010. Anisotropic and hyperelastic identification of in vitro human arteries from full-field optical measurements. Journal of biomechanics. 43(15):2978–85. Available from: `http://www.ncbi.nlm.nih.gov/pubmed/20673669`.

Badel P, Avril S, Lessner S, Sutton M. 2011. Mechanical identification of hyperelastic anisotropic properties of mouse carotid arteries. Mechanics of Biological Systems and Materials. 2(c):11–17. Available from: `http://www.springerlink.com/index/10.1007/978-1-4614-0219-0`.

Badel P, Rohan CPY, Avril S. 2013. Finite Element simulation of buckling-induced vein tortuosity and influence of the wall constitutive properties. Journal of the Mechanical Behavior of Biomedical Materials. 26:119–126.

Bellini C, Glass P, Sitti M, Di Martino ES. 2011. Biaxial mechanical modeling of the small intestine. Journal of the mechanical behavior of biomedical materials. 4(8):1727–40. Available from: `http://www.ncbi.nlm.nih.gov/pubmed/22098873`.

Bucchi A, Hearn GE. 2013a. Predictions of aneurysm formation in distensible tubes: Part A Theoretical background to alternative approaches. International Journal of Mechanical Sciences. 71:1–20. Available from: `http://linkinghub.elsevier.com/retrieve/pii/S0020740313000593`.

Bucchi A, Hearn GE. 2013b. Predictions of aneurysm formation in distensible tubes: Part B Application and comparison of alternative approaches. International Journal of Mechanical Sciences. 70:155–170. Available from: `http://linkinghub.elsevier.com/retrieve/pii/S0020740313000702`.

Chuong CJ, Fung YC. 1986. On Residual Stresses in Arteries. Journal of Biomechanical Engineering. 108(2):189. Available from: `http://biomechanical.asmedigitalcollection.asme.org/article.aspx?articleid=1397297`.

Crisfield M. 1981. A fast incremental/iterative solution procedure that handles snap-through. Computers & Structures. 13(1-3):55–62. Available from: `http://www.sciencedirect.com/science/article/pii/0045794981901085`.

Dassault Systèmes S. 2014. Abaqus Analysis User's Guide.

de Gelidi S. 2016. Investigation of aneurysm formation : a macro-structural approach [dissertation]. University of Portsmouth. Available from: `https://ethos.bl.uk/OrderDetails.do?uin=uk.bl.ethos.714173`.

de Gelidi S, Tozzi G, Bucchi A. 2017. The effect of thickness measurement on numerical arterial models. Materials Science & Engineering C. 76:1205–1215.

Delfino a, Stergiopulos N, Moore JE, Meister JJ. 1997. Residual strain effects on the stress field in a thick wall finite element model of the human carotid bifurcation. Journal of biomechanics. 30(8):777–786.

Deplano V, Boufi M, Boiron O, Guivier-Curien C, Alimi Y, Bertrand E. 2016. Biaxial tensile tests of the porcine ascending aorta. Journal of Biomechanics. 49:2031–2037.

Doyle BJ, Callanan A, McGloughlin TM. 2007. A comparison of modelling techniques for computing wall stress in abdominal aortic aneurysms. Biomedical engineering online. 6:38. Available from: `http://www.pubmedcentral.nih.gov/articlerender.fcgi?artid=2169238{&}tool=pmcentrez{&}rendertype=abstract`.

Doyle BJ, Corbett TJ, Callanan A, Walsh MT, Vorp DA, McGloughlin TM. 2009. An experimental and numerical comparison of the rupture locations of an abdominal aortic aneurysm. Journal of endovascular therapy: an official journal of the International Society of Endovascular Specialists. 16(3):322–35. Available from: `http://www.pubmedcentral.nih.gov/articlerender.fcgi?artid=2795364{&}tool=pmcentrez{&}rendertype=abstract`.

Drake R, Vogl W, Mitchell A, Gray H. 2010. Gray's anatomy for students. 2nd ed. Philadelphia: Churchill Livingstone.

Fan R, Sacks MS. 2014. Simulation of planar soft tissues using a structural constitutive model: Finite element implementation and validation. Journal of Biomechanics. 47(9):2043–2054. Available from: `http://dx.doi.org/10.1016/j.jbiomech.2014.03.014`.

Fehervary H, Smoljkic M, Vander Sloten J, Famaey N. 2016. Planar biaxial testing of soft biological tissue: a critical analysis of protocol and fitting process. Journal of the mechanical behavior of biomedical materials. 61:135–151.

Fu YB, Pearce SP, Liu KK. 2008. Post-bifurcation analysis of a thin-walled hyperelastic tube under inflation. International Journal of Non-Linear Mechanics. 43(8):697–706.

Fu YB, Rogerson G, Zhang Y. 2012. Initiation of aneurysms as a mechanical bifurcation phenomenon. International Journal of Non-Linear Mechanics. 47(2):179–184. Available from: `http://linkinghub.elsevier.com/retrieve/pii/S0020746211000990`.

Fung YC. 1993. Biomechanics: Mechanical Properties of Living Tissues. New York: Springer. Available from: `http://books.google.com/books?id=4HaMStTGOHwC{&}pgis=1`.

Fung YC, Fronek K, Patitucci P. 1979. Pseudoelasticity of arteries and the choice of its mathematical expression Pseudoelasticity of arteries and the choice of its mathematical expression of Applied Mechanics. The American Physiological Society. 237:H620–H631.

Gasser CT, Auer M, Labruto F, Swedenborg J, Roy J. 2010. Biomechanical rupture risk assessment of abdominal aortic aneurysms: model complexity versus predictability of finite element simulations. European journal of vascular and endovascular surgery: the official journal of the European Society for Vascular Surgery. 40(2):176–85. Available from: `http://www.sciencedirect.com/science/article/pii/S1078588410002364`.

Georgakarakos E, Ioannou CV, Kamarianakis Y, Papaharilaou Y, Kostas T, Manousaki E, Katsamouris AN. 2010. The Role of Geometric Parameters in the Prediction of Abdominal Aortic Aneurysm Wall Stress. European Journal of Vascular and Endovascular Surgery. 39(1):42–48. Available from: `http://dx.doi.org/10.1016/j.ejvs.2009.09.026`.

Giannakoulas G, Giannoglou G, Soulis J, Farmakis T, Papadopoulou S, Parcharidis G, Louri-

das G. 2005. A computational model to predict aortic wall stresses in patients with systolic arterial hypertension. Medical Hypotheses. 65(6):1191–1195.

Giannoglou G, Giannakoulas G, Soulis J, Chatzizisis Y, Perdikides T, Melas N, Parcharidis G, Louridas G. 2006. Predicting the Risk of Rupture of Abdominal Aortic Aneurysms by Utilizing Various Geometrical Parameters: Revisiting the Diameter Criterion. Angiology. 57(4):487–494. Available from: `http://ang.sagepub.com/cgi/doi/10.1177/0003319706290741`.

Han HC. 2007. A Biomechanical Model of Artery Buckling. Journal of biomechanics. 40(16):3672–3678.

Holzapfel GA. 2006. Determination of material models for arterial walls from uniaxial extension tests and histological structure. Journal of theoretical biology. 238(2):290–302. Available from: `http://www.ncbi.nlm.nih.gov/pubmed/16043190`.

Holzapfel GA, Gasser CT, Ogden RW. 2000. A new constitutive framework for arterial wall mechanics and a comperative study of material models. Journal of Elasticity. 61:1–48.

Holzapfel GA, Gasser CT, Ogden RW. 2004. Comparison of a multi-layer structural model for arterial walls with a fung-type model, and issues of material stability. Journal of biomechanical engineering. 126(April):264–275.

Horgan CO, Murphy JG. 2010. Simple shearing of incompressible and slightly compressible isotropic nonlinearly elastic materials. Journal of Elasticity. 98(2):205–221.

Horný L, Netusil M, Vonavkova T. 2014. Axial prestretch and circumferential distensibility in biomechanics of abdominal aorta. Biomechanics and Modeling in Mechanobiology. 13(4):783–799.

Horný L, Žitný R, Chlup H, Macková H. 2006. Identification of the material parameters of an aor- tic wall. Bulletin of Applied Mechanics. 2(8):173–181.

Isaksen JG, Bazilevs Y, Kvamsdal T, Zhang Y, Kaspersen JH, Waterloo K, Romner B, Ingebrigtsen T. 2008. Determination of wall tension in cerebral artery aneurysms by numerical simulation. Stroke. 39:3172–3178.

Koseki H, Miyata H, Shimo S, Ohno N, Mifune K, Shimano K, Yamamoto K, Nozaki K, Kasuya H, Narumiya S, et al. 2019. Two Diverse Hemodynamic Forces, a Mechanical Stretch and a High Wall Shear Stress, Determine Intracranial Aneurysm Formation. Translational Stroke Research:1–13. Available from: `http://link.springer.com/10.1007/s12975-019-0690-y`.

Labrosse MR, Beller CJ, Mesana T, Veinot JP. 2009. Mechanical behavior of human aortas: Experiments, material constants and 3-D finite element modeling including residual stress. Journal of Biomechanics. 42(8):996–1004.

Lee AY, Sanyal A, Xiao Y, Shadfan R, Han HC. 2014. Mechanical instability of normal and aneurysmal arteries. Journal of Biomechanics. 47(16):3868–3875. Available from: `http://linkinghub.elsevier.com/retrieve/pii/S0021929014005296`.

Ma B, Lu J, Harbaugh RE, Raghavan ML. 2007. Nonlinear anisotropic stress analysis of anatomically realistic cerebral aneurysms. Journal of biomechanical engineering. 129(February 2007):88–96.

Maher E, Creane A, Lally C, Kelly DJ. 2012. An anisotropic inelastic constitutive model to describe stress softening and permanent deformation in arterial tissue. Journal of the mechanical behavior of biomedical materials. 12:9–19. Available from: `http://www.ncbi.nlm.nih.gov/pubmed/22659364`.

Marlow RS. 2003. A general first-invariant hyperelastic constitutive model. In: Busfield JJC, Muhr AH, editors. Constitutive models for rubber iii. Lisse: Taylor & Francis; p. 157–160.

NHS. 2017. Abdominal aortic aneurysm - Treatment. [accessed 2014-10-03]. Available from: `http://www.nhs.uk/Conditions/repairofabdominalaneurysm/Pages/Treatment.aspx`.

NHS. 2019. High blood pressure (hypertension). [accessed 2019-06-03]. Available from: `https://www.nhs.uk/conditions/high-blood-pressure-hypertension/`.

Noordergraaf A. 1956. Physical Basis of Ballistocardiography. S-Gravenhage: Excelsior. Available from: `https://books.google.co.uk/books/about/Physical{_}Basis{_}of{_}Ballistocardiography.html?id=0uG4GQAACAAJ{&}pgis=1`.

Nunes LCS, Moreira DC. 2013. Simple shear under large deformation: Experimental and theoretical analyses. European Journal of Mechanics, A/Solids. 42:315–322. Available from: `http://dx.doi.org/10.1016/j.euromechsol.2013.07.002`.

Ogden RW. 1972. Large deformation isotropic elasticity - on the correlation of theory and experiment for incompressible rubberlike solids. Royal society. 326(1567):565–584.

Ogden RW. 1997. Non-linear Elastic Deformations. Dover Publications. Available from: `https://books.google.com/books?id=gPUMmyYdNIgC{&}pgis=1`.

Pandit A, Lu X, Wang C, Kassab GS. 2005. Biaxial elastic material properties of porcine coronary media and adventitia. American journal of physiology Heart and circulatory physiology. 288(6):H2581–H2587. Available from: `http://www.ncbi.nlm.nih.gov/pubmed/15792993`.

Public Health England. 2019. AAA screening annual data published for 2017 to 2018. [accessed 2019-06-03]. Available from: `https://phescreening.blog.gov.uk/2019/01/31/aaa-screening-annual-data-published-for-2018-to-2018/`.

Rachev A. 2009. A theoretical study of mechanical stability of arteries. Journal of biomechanical engineering. 131(5):051006 1–10.

Raghavan ML, Vorp DA. 2000. Toward a biomechanical tool to evaluate rupture potential of abdominal aortic aneurysm : identification of a finite strain constitutive model and evaluation of its applicability. Journal of Biomechanics. 33:475–482.

Ramachandran M, Laakso A, Harbaugh RE, Raghavan ML. 2012. On the role of modeling choices in estimation of cerebral aneurysm wall tension. Journal of Biomechanics. 45(16):2914–2919.

Riks E. 1979. An incremental approach to the solution of snapping and buckling problems. International Journal of Solids and Structures. 15(7):529 – 551.

Rodríguez JF, Merodio J. 2011. A new derivation of the bifurcation conditions of inflated cylindrical membranes of elastic material under axial loading. Application to aneurysm formation. Mechanics Research Communications. 38(3):203–210. Available from: `http://www.sciencedirect.com/science/article/pii/S0093641311000309`.

Rodríguez JF, Ruiz C, Doblaré M, Holzapfel GA. 2008. Mechanical stresses in abdominal aortic aneurysms: influence of diameter, asymmetry, and material anisotropy. Journal of biomechanical engineering. 130(2):021023 1–10.

Schmidt T, Pandya D, Balzani D. 2015. Influence of isotropic and anisotropic material models on the mechanical response in arterial walls as a result of supra-physiological loadings. Mechanics Research Communications. 64:29–37. Available from: `http://linkinghub.elsevier.com/retrieve/pii/S009364131400158X`.

Schulze-Bauer CaJ, Holzapfel GA. 2003. Determination of constitutive equations for human arteries from clinical data. Journal of biomechanics. 36(2):165–9. Available from: `http://www.ncbi.nlm.nih.gov/pubmed/12547353`.

Schulze-Bauer CaJ, Regitnig P, Holzapfel GA. 2002. Mechanics of the human femoral adventitia including the high-pressure response. American journal of physiology Heart and circulatory physiology. 282(6):H2427–H2440.

Scotti CM, Jimenez J, Muluk SC, Finol EA. 2008. Wall stress and flow dynamics in abdominal aortic aneurysms: finite element analysis vs. fluid-structure interaction. Computer methods in biomechanics and biomedical engineering. 11(3):301–322. Available from: `http://www.ncbi.nlm.nih.gov/pubmed/18568827`.

Shang EK, Nathan DP, Woo EY, Fairman RM, Wang GJ, Gorman RC, Gorman JH, Jackson BM. 2015. Local wall thickness in finite element models improves prediction of abdominal aortic aneurysm growth. Journal of Vascular Surgery. 61(1):217–223. Available from: `http://dx.doi.org/10.1016/j.jvs.2013.08.032`.

Signorelli F, Sela S, Gesualdo L, Chevrel S, Tollet F, Pailler-Mattei C, Tacconi L, Turjman F, Vacca A, Schul DB. 2018. Hemodynamic Stress, Inflammation, and Intracranial Aneurysm Development and Rupture: A Systematic Review. World Neurosurgery. 115:234–244.

Sommer G, Sherifova S, Oberwalder PJ, Dapunt OE, Ursomanno PA, DeAnda A, Griffith BE, Holzapfel GA. 2016. Mechanical strength of aneurysmatic and dissected human thoracic aortas at different shear loading modes. Journal of Biomechanics. 49(12):2374–2382. Available

from: `http://linkinghub.elsevier.com/retrieve/pii/S0021929016302238`.

Sun W, Sacks MS. 2005. Finite element implementation of a generalized Fung-elastic constitutive model for planar soft tissues. Biomechanics and modeling in mechanobiology. 4(2-3):190–199. Available from: `http://www.ncbi.nlm.nih.gov/pubmed/16075264`.

Sun W, Sacks MS, Scott MJ. 2005. Effects of Boundary Conditions on the Estimation of the Planar Biaxial Mechanical Properties of Soft Tissues. Journal of Biomechanical Engineering. 127:709 – 715. Available from: `http://biomechanical.asmedigitalcollection.asme.org/article.aspx?articleid=1414532`.

Takizawa K, Christopher J, Tezduyar TE, Sathe S. 2010. Spacetime finite element computation of arterial fluidstructure interactions with patient-specific data. International Journal for Numerical Methods in Biomedical Engineering. 26:101–116. Available from: `http://onlinelibrary.wiley.com/doi/10.1002/cnm.1494/full`.

Vaishnav RN, Vossoughi J. 1987. Residual stress and strain in aortic segments. Journal of Biomechanics. 20(3):235–239. Available from: `http://www.sciencedirect.com/science/article/pii/0021929087902909`.

Vande Geest JP, Sacks MS, Vorp DA. 2006. The effects of aneurysm on the biaxial mechanical behavior of human abdominal aorta. Journal of biomechanics. 39(7):1324–1334. Available from: `http://www.ncbi.nlm.nih.gov/pubmed/15885699`.

Vossoughi J, Tözeren A. 1998. Determination of an effective shear modulus of aorta. Russian Journal of Biomechanics. 12:20–36.

Vychytil J, Moravec F, Kochová P, Kuncová J, Švíglerová J. 2010. Modelling of the mechanical behaviour of porcine carotid artery undergoing inflation-deflation test. Applied and computational mechanics. 4:251–262. Available from: `https://otik.uk.zcu.cz/handle/11025/1405`.

Wang DHJ, Makaroun MS, Webster MW, Vorp DA. 2002. Effect of intraluminal thrombus on wall stress in patient-specific models of abdominal aortic aneurysm. Journal of vascular surgery. 36(3):598–604.

Wang JJ, Parker KH. 2004. Wave propagation in a model of the arterial circulation. Journal of biomechanics. 37(4):457–70. Available from: `http://www.ncbi.nlm.nih.gov/pubmed/14996557`.

Wang X, Li X. 2011. Fluid-structure interaction based study on the physiological factors affecting the behaviors of stented and non-stented thoracic aortic aneurysms. Journal of Biomechanics. 44(12):2177–2184. Available from: `http://dx.doi.org/10.1016/j.jbiomech.2011.06.020`.

Westerhof N, Bosman F, De Vries CJ, Noordergraaf A. 1969. Analog studies of the human systemic arterial tree. Journal of Biomechanics. 2(2):121–143. Available from: `http://www.jbiomech.com/article/0021929069900244/fulltext`.

Yeoh OH. 1993. Some forms of the strain energy function for rubber. Rubber Chemistry and Technology. 66:754–771.

Zhou J, Fung YC. 1997. The degree of nonlinearity and anisotropy of blood vessel elasticity. Proceedings of the National Academy of Sciences of the United States of America. 94(26):14255–14260.
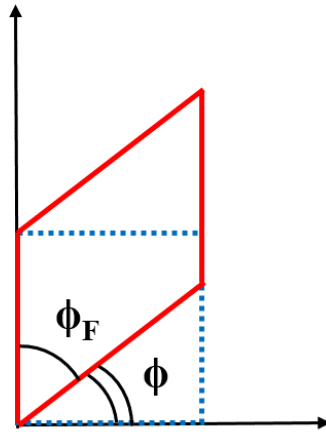
List of Figures

Figure A1. Sketch of a simple shear test transforming the original configuration (dashed blue) into the deformed one (red). The angle ϕ_F is needed to calculate Green-Lagrange shear strain